Simulation of journal bearing friction in severe mixed lubrication – Validation and effect of surface smoothing due to running-in

D.E. Sander*, H. Allmaier†, H.H. Priebsch‡, M. Witt§, A. Skiadas¶

December, 2015

Abstract

This paper focuses on the friction behavior of journal bearings operating from hydrodynamic to mixed lubrication regime where severe metal-metal contact occurs. Therefore, friction tests with two different static loads are carried out on the journal bearing test-rig from KS Gleitlager. The test results in form of Stribeck curves provide a solid base to proof the isothermal elastohydrodynamic simulation approach. The simulation approach solves the averaged Reynolds equation introduced by Patir and Cheng and considers metal-metal contact by using the Greenwood and Tripp contact model. All necessary surface parameters are derived from surface scans. No less essential in this approach are the experimentally identified lubricant properties under high pressure and high shear rate.

The calculated friction torque matches the measurement results within the measurement uncertainty for a wide range of operation conditions. With the validated simulation approach the influence of surface smoothing due to metal-metal contact is discussed. Additionally, the limits of a constant boundary coefficient are identified and the effects of flow factors are presented.

*VIRTUAL VEHICLE Research Center, Austria
†VIRTUAL VEHICLE Research Center, Austria
‡VIRTUAL VEHICLE Research Center, Austria
§KS Gleitlager GmbH, Am Bahnhof 14, 68789 St. Leon-Rot, Germany
¶KS Gleitlager GmbH, Am Bahnhof 14, 68789 St. Leon-Rot, Germany

1 Introduction

The mixed lubrication regime describes the transition between the pure hydrodynamic lubrication regime, where a fluid separates the contacting surfaces and the boundary lubrication regime, where metal-metal contact is leading. Characteristically for the mixed lubrication regime is that the fluid film cannot completely separate the adjacent surfaces and single asperities interact. Hence, the friction in mixed lubrication regime (mixed friction) is characterized by the co-existence of hydrodynamic and asperity friction [1]. The friction coefficient finds its minimum between the pure hydrodynamic lubrication and the mixed lubrication. In terms of friction reduction and efficiency it is beneficial to operate lubricated contacts in this condition. Unfortunately, wear occurs as asperities are in contact and durability problems can occur.

Especially in the automotive sector a trend to cut fuel consumption and emissions has been established which is driven by emission regulations and customer satisfaction. Downscaled turbocharged combustion engines with high power density are an achievement in modern engine development for performance improvement. The high power and small dimensions of engine components lead to highly loaded lubricated contacts such as journal bearings. Another efficiency benefit is pledged to friction reduction with low-viscous lubricants. These advancements lead to a decreasing oil film thickness in lubricated contacts. This means that journal bearings, which formerly mainly ran in pure hydrodynamic lubrication regime to ensure a long lifetime, may partly expose metal-

metal contact during the dynamic operation [2, 3, 4].

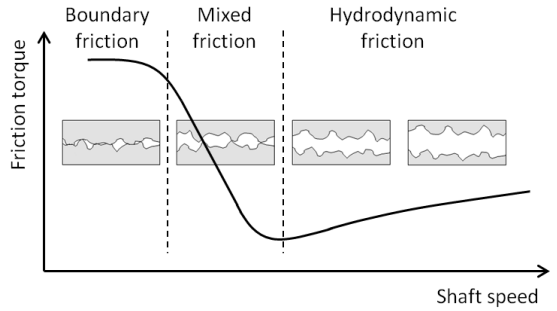

Figure 1: Sketch of a Stribeck curve with different lubrication regimes

For lubricated contacts, and particularly for journal bearings the Stribeck curve (see figure 1), named after Richard Stribeck [5, 6], has became a common tool to assess friction benefits. A static load is applied to the journal bearing and the friction torque is measured for a wide speed range. With such a test configuration the different lubrication regimes can be identified. Bovington [7] describes the importance of the Stribeck curve in bearing design and discusses the effect of low-viscosity lubricant and oil additives. He conducted several tests with various engine oils which were formulated differently. More recently, the influence of surface dimple effects on journal bearing friction are experimentally studied [8] by evaluating the Stribeck curve. In the present study, a similar test setup is used for the measurements. The experimental results in form of Stribeck curves provide a solid base to validate the simulation approach.

Predictive simulation approaches to describe lubricated contacts in journal bearings are broadly discussed in literature and differ in their level of detail. An overview of elastohydrodynamic lubrication analysis of conformal contacts without metal-metal contact is given by Booker et al. [9]. The extensive review focuses on the 2D Reynolds equation and discusses, among other things, bearing deformation, mass-conservative cavitation and pressure-viscosity effects. Also, the effect of surface roughness on bearing performance in elastohydrodynamic lubrication is discussed. Dobrica et al. [10] compare stochastic and deterministic models in more detail and conclude that the stochastic model correctly anticipate the trends of the deterministic models for the investigated surfaces. Both studies don't consider slip boundary conditions which is recently reviewed and discussed by Jao et al. [11]. Beyond the scope of this study is the 3D consideration of the fluid film using a computational fluid dynamics (CFD) approach [12]. Recently, Shahmohamadi et al. [13] present a thermohydrodynamic analysis using CFD approach including a vapour transport equation to consider cavitation. Both, temperature and pressure distribution agree well with experimental data.

However, the interaction of single asperities between the contacting surfaces occur in mixed lubrication regime and have an impact on journal bearing performance. Simulation approaches considering the asperity contact in journal bearings are covered in many text books, for instance [14, 15, 16]. Therefore, an extensive reference list is not replicated here.

Notably, only a minor number of publications discuss journal bearing friction in severe mixed lubrication and verify the calculated results with measurement results. Bartel et al. [17] present an analytical model considering metal-metal contact by using an energy approach. The calculated results were compared to measured Stribeck curves. The authors conclude that the viscosity-pressure behavior has a huge influence on the results and should not be neglected. Further, macro-deformation of shaft and bearing need to be considered for realistic friction prediction. Lu et al. [18] present a simple theoretical analysis for friction prediction in mixed and boundary lubrication regime and verified the analysis for different loads and temperatures. The tool is also used to investigate the effect of surface pattern and asperity orientation on Stribeck curves [19].

Wang et al. [20] present an analytical method to derive Stribeck curves and discuss the influence of roughness, elasticity, and thermoelasticity on friction. Especially the elastic deformation has a strong influence on the friction behavior. The influence of surface adaption caused by running-in wear on friction in dynamically loaded bearings is discussed by Bar-

tel et al. [21]. Beside the change of surface roughness an adaption of the bearing geometry is calculated. A clear reduction of maximum contact pressure and friction is identified for the worn bearing. The influence of a worn geometry on journal bearing performance is also discussed by investigating misaligned bearings [22] and bearings subjected to numerous starts and stops [23]. Both papers conclude that a worn bearing geometry decreases the bearing temperatures. Sun et al. [24] calculate the effect of surface roughness change on misaligned journal bearings and highlights the importance of elastically deformation of the contacting bodies. However, no contact model is implemented to discuss friction due to asperity interaction.

The present study focuses on friction losses in journal bearings operating in severe mixed lubrication regime. The analytical investigation uses an isothermal mixed elastohydrodynamic simulation approach which considers the elastic deformation of shaft and bearing structure. Although the temperature is assumed to be constant within the bearing, the variation between different loads and shaft speeds is considered with introducing an equivalent bearing temperature. The equivalent bearing temperature is derived from temperature measurements at the back of the bearing shells. Additionally, the piezoviscous and non-Newtonian behavior of the lubricant are included in the approach. The equation describing the lubricant viscosity is dependent on temperature, pressure and shear rate and was previously derived by measurement. The detailed derivation of the viscosity equation was published in [25] and validated for dynamically loaded journal bearings operating in mainly hydrodynamic regime.

The influence of asperities on hydrodynamic friction is included by using the flow factors according to Patir and Cheng [26, 27]. Friction due to metal-metal contact is considered by the Greenwood and Tripp contact model [28]. To derive the parameters for both, flow factors and contact model, bearing shell surface and shaft surface were scanned by white light interferometry. From the surface scans roughness parameters and asperity orientation are established. The boundary friction coefficient is the remaining unknown parameter which is chosen to be constant in this work.

Primary aim of this study is the validation of the simulation approach to calculate journal bearing friction in severe mixed lubrication regime. Further, the practicability and limits of the simple elastic Greenwood-Tripp contact model in combination with a constant boundary friction coefficient is discussed.

For a secondary aim, the influence of surface smoothing due to running-in on friction in mixed lubrication is discussed. Therefore, a ran-in journal bearing surface is analyzed and a second contact model is derived. The influence on metal-metal contact pressure, minimum radial clearance and friction is analyzed.

Further, the exclusion of the flow factors from the simulation and its effect on journal bearing friction is discussed.

Moreover, the presented study complements previous research by the authors which focused on journal bearing friction excited by dynamic loads. Allmaier et al. [29, 30] presented a simulation approach using an isothermal bearing assumption. He included the viscosity-pressure relation for different single-grade lubricants and validated the friction losses over a wide range of operation conditions. Metal-metal contact was identified by simulation and also by measuring the contact voltage [31]. Later, the isothermal model was extended to a thermo-elastohydrodynamic model [32] which is able to predict the measured temperatures at the bearing shell. The results also justified the usage of an isothermal simulation approach in terms of friction prediction. Sander et al. [25] included the non-Newtonian behavior of modern multigrade engine oils into the isothermal simulation approach. Again, the simulation results were validated for a variety of shaft speeds and dynamic loads up to 100 MPa specific load in the test bearing. After the test procedure worn areas on the bearing surface were identified which was caused by metal-metal contact. Metal-metal contact was also identified by simulation. As a consequence research on the running in process of journal bearings was conducted [33, 34]. Complementary, the presented results are obtained from the same simulation approach yet discuss friction in severe mixed lubrication regime.

2 Lubricant properties

The lubricant's viscosity is directly related to the friction in hydrodynamic lubrication regime. In mixed lubrication regime the lubrication additives modifies the frictional behavior of the contacting surfaces. It is thus important to explicitly describe the lubricant.

In this work a fully formulated low viscous 0W20 hydrocarbon engine oil is used as it is available on the automotive market. The main properties of the modern lubricant including the density and the viscosity at various conditions are given in table 1.

Table 1: Basic properties of the tested 0W20 lubricant

Density at 40 °C	832.5	kg/m^3
Dyn. viscosity 40 °C	37.5	mPas
Dyn. viscosity 100 °C	6.8	mPas
HTHS-viscosity[1]	2.7	mPas

Additionally to the temperature dependency of the rheological properties, the viscosity is strongly dependent on pressure and shear rate. Therefore, the piezoviscous and the non-Newtonian behavior of the lubricant were analyzed. In previous publication by the authors [25] the parameters (see table 2) for the empirical viscosity equation according to Vogel [35], Barus [36] and Cross [37] were derived from experimental data:

$$\eta(T,p,\dot{\gamma}) = A \cdot e^{\frac{B}{(T+C)}+\alpha \cdot p} \cdot \left(r + \frac{1-r}{1+(K\cdot\dot{\gamma})^m} \right) \quad (1)$$

In the simulation the viscosity is represented by equation (1). The corresponding values are listed in table 2.

Table 2: Parameters for Eqs. (1) derived from experimental data [25]

A	0.0516	mPas
B	1127.6	°C
C	130.7	°C
α	0.00095	1/bar
r	0.53	-
m	0.79	-
K	7.9 e-8	s

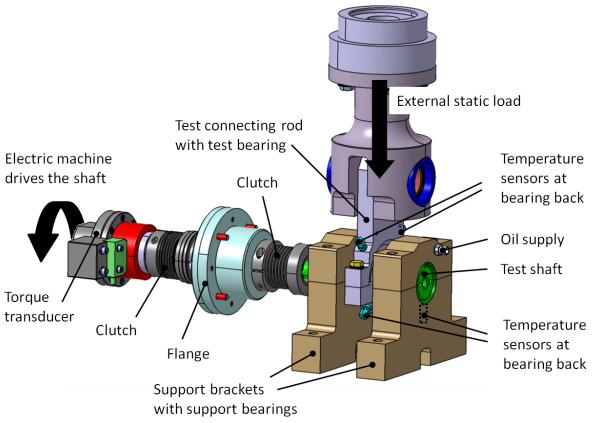

Figure 2: Journal bearing test-rig at KS Gleitlager

3 Testing

The journal bearing test-rig at KS Gleitlager was used to perform the experimental friction measurement. The test-rig is sketched in figure 2.

[1] The HTHS-viscosity is defined as the viscosity at high temperature (150 °C) and high shear rate (10^6 1/s).

It consists of a rotating straight shaft which rests on two supporting journal bearings in support brackets. The shaft is driven by an elastically clutched electric motor. A test connecting rod is placed in between the two support brackets. An external load is applied onto the test connecting rod and on to the test journal bearing. The test journal bearing has a diameter of 47.8 mm and a width of 17.2 mm and corresponds to a typical big-end bearing used in modern combustion engine. The preconditioned oil is supplied through a hole in the lower bearing shell which. Both support journal bearings have a diameter of 54 mm and a width of 25 mm. It has an 180° oil supply grove all along the top shell. All three bearings are made of a steel-aluminum composite material.

The test rig is equipped with a torque transducer, a Manner Sensortelemetrie 50 N m with an accuracy of ±0.15 N m. The transducer is placed between the electric motor and the shaft to measure the friction torque generated by all three bearings. The bearing temperatures were monitored during the test. Therefore, PT100 elements were placed at the back of the bearing shells. The elements have an accuracy of ±0.5 °C.

3.1 Test conditions

For the investigation of friction in mixed lubrication regime a static load is applied to the test connecting rod. Hence, only the top shell of the test bearing and the bottom shell of the support bearings are stressed. Further the oil is supplied via the unloaded bearing shells. Two load cases are investigated, the first with 8 kN load and the second with a 4 kN load which correspond to 10 MPa specific load in the test bearing and 5 MPa, respectively. In the beginning of each test new bearing shells are placed into the test connecting rod and the support brackets. One test run consists of a constant speed-up to 6000 rpm followed by a constant speed-down until the shaft stops to rotate. One test run lasts for 12 min. The second half in other words, the speed-down is recorded and evaluated. The shaft speed during the speed-down is plotted in figure 3 over time (dashed black line).

The lubricant which is supplied to all three bearings is preconditioned during the entire test procedure. Hence, the lubricant supply temperature stays stable between 91 °C and 92 °C during the test run and is similar for both load cases. The black solid curve in figure 3 shows the supply temperature for 10 MPa load and the grey solid curve represents the supply temperature for 5 MPa load.

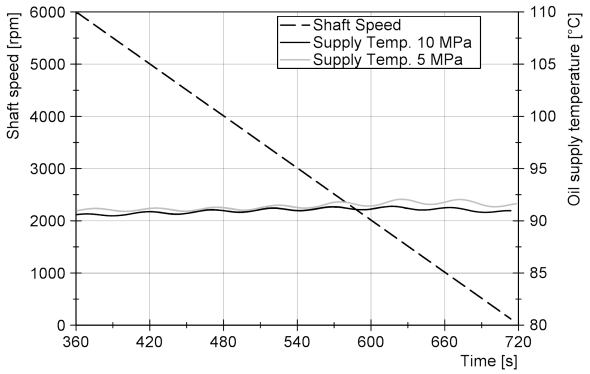

Figure 3: Shaft speed (black dashed curve) and oil supply temperature (black and grey solid curve) over time

3.2 Test results

The measured overall friction torque is shown in figure 4 over the shaft speed for both load cases.

The black curve represents the measured friction torque under the specific static load of 10 MPa. At a shaft speed of 6000 rpm the friction torque is 1.6 N m. By reducing the shaft speed the friction moment decreases to a minimum of 0.5 N m at around 400 rpm. Below 400 rpm the friction moment abruptly increases. At high speed the bearing operates in hydrodynamic lubrication regime. The rise of the friction torque below 400 rpm is attributed to metal-metal contact between the shaft and bearing shell. The grey curve shows the friction torque measured with an applied load of 5 MPa. Compared to the 10 MPa load case, a lower friction torque can be identified all over the investigated speed range. In the hydrodynamic

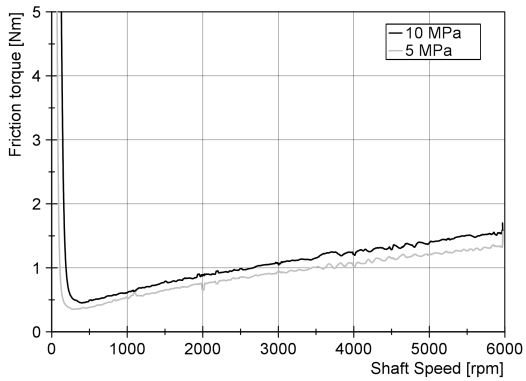

Figure 4: Friction torque over shaft speed for 10 MPa static load (black) and 5 MPa static load (grey)

regime the friction torque is reduced by around 15 %.

4 Simulation

For the simulation the KS Gleitlager test rig is modeled within the flexible multi-body solver AVL Excite Power Unit[2] [38, 39]. The test shaft, the test connecting rod and the two support brackets are represented as mathematical condensed finite element structures which can deform elastically [40]. The lubricated journal bearings which connect the components are calculated by solving the Reynolds equation by finite volume approach [38]. The discretization points of the lubrication regime are equally distributed along the axial and circumferential direction. In the presented model 25 points in axial direction are chosen for all bearings. In circumferential direction the test bearing has 200 points and the support bearing has 176 points. Every second point is directly coupled to a point on the solid structure. The displacement of the points in between are interpolated. The coupling method is described in [41]. When the distance between the facing surfaces decreases their surface roughness will affect the oil flow.

[2]Version 2014.1, AVL List GmbH, Advanced Simulation Technology, Hans-List-Platz 1, 8020 Graz Austria, www.avl.com

Patir and Cheng [26, 27] introduced flow factors to the Reynolds equation taking this influence into account:

$$-\frac{\partial}{\partial x}\left(\phi_{\mathrm{x}}\frac{h^3}{12\eta}\frac{\partial p}{\partial x}\right)-\frac{\partial}{\partial y}\left(\phi_{\mathrm{y}}\frac{h^3}{12\eta}\frac{\partial p}{\partial y}\right)+ \\ +\frac{\partial}{\partial x}\left(h\frac{u_1+u_2}{2}\right)+\frac{\partial}{\partial x}\left(\phi_{\mathrm{s}}\frac{u_1+u_2}{2}\sigma_s\right)+\frac{\partial h}{\partial t}=0, \tag{2}$$

where x, y denote the circumferential and the axial direction, respectively. p is the hydrodynamic pressure and h the oil film thickness which is dependent on x and y. Further, u_1 and u_2 denote the sliding speeds of the facing surfaces. The influence of surface roughness is considered by the pressure flow factors ϕ_{x}, ϕ_{y} and the shear flow factor ϕ_{s}. The oil viscosity η is considered temperature, pressure and shear rate dependent in this paper (see equation 1).

The consideration of the asperity contact itself is described below (see section 4.2). The cavitation model is based on the JFO approach [42, 41]. However, the non-linear model is solved in time domain. Therefore, each simulation runs until a stable quasi-static condition is achieved.

4.1 Friction Moment

The friction torque acting on the bearing surface considers both, hydrodynamic losses and losses due to asperity contact. Therefore, the friction torque M_{Friction} can be calculated by integrating the shear stresses over the bearing surface:

$$M_{\mathrm{Friction}} = r\iint_A (\tau_h+\tau_a)\,dxdy, \tag{3}$$

where A denotes the bearing surface and r is the nominal shell radius. τ_h is the hydrodynamic shear stress. It is calculated by

$$\tau_h = \eta\cdot\frac{u_1-u_2}{h}(\phi_{\mathrm{f}}\pm\phi_{\mathrm{fs}})\pm\phi_{\mathrm{fp}}\frac{h}{2}\cdot\frac{\partial p}{\partial x}, \tag{4}$$

where $+$ and $-$ refer to the shell surface and the journal surface, respectively. ϕ_{f}, ϕ_{fs} and ϕ_{fp} are the shear stress factors according to Patir and Cheng.

The shear stress in case of asperity contact τ_a between the shell surface and the journal surface is calculated by

$$\tau_a = \mu_{\text{Bound}} \cdot p_a, \tag{5}$$

where μ_{Bound} is the boundary friction coefficient and p_a denotes the asperity contact pressure.

4.2 Asperity contact pressure

The asperity contact pressure is calculated using the Greenwood and Tripp approach [43, 28]. The theory of Greenwood and Tripp is based on the contact of two nominally flat, random rough surfaces. The asperity contact pressure can be written as

$$p_{\text{a}} = KE^* F_{\frac{5}{2}}(H_s), \tag{6}$$

where E^* is the composite elastic modulus, $E^* = (\frac{1-\nu_1^2}{E_1} + \frac{1-\nu_2^2}{E_2})^{-1}$, where ν_i and E_i are the Poisson ratio and Young's modulus of the adjacent surfaces, and $F_{\frac{5}{2}}(H_s)$ is the form function, which is defined as

$$F_{\frac{5}{2}}(H_s) = \begin{cases} 4.4086 \cdot 10^{-5}(4 - H_s)^{6.804}, & \text{if } H_s < 4 \\ 0, & \text{if } H_s \geq 4 \end{cases} \tag{7}$$

H_s is a dimensionless clearance parameter, defined as $H_s = (h - \overline{\delta}_s)/\sigma_s)$, with σ_s being the combined asperity summit roughness, which is calculated according to

$$\sigma_s = \sqrt{\sigma_{s,J}^2 + \sigma_{s,S}^2} \tag{8}$$

and $\overline{\delta}_s$ being the combined mean summit height, $\overline{\delta}_s = \overline{\delta}_{s,J} + \overline{\delta}_{s,S}$. The form factor $F_{\frac{5}{2}}(H_s)$ becomes zero for a dimensionless clearance parameter beyond four which further means no asperity contact occurs. Finally, the elastic factor K is defined as

$$K = \frac{16 \cdot \sqrt{2} \cdot \pi}{15} \cdot (\sigma_s \cdot \overline{\beta}_s \cdot \eta_s)^2 \cdot \sqrt{\frac{\sigma_s}{\overline{\beta}_s}}, \tag{9}$$

where $\overline{\beta}_s$ is the mean summit radius and η_s is the summit density.

4.3 Bearing temperatures

The lubricant temperature within the journal bearing varies according to the local position. For the simulation, an equivalent bearing temperature is introduced to consider the temperature as constant in the lubrication gap. For each speed the equivalent temperature is calculated from the measured bearing back temperatures. The approach is described in [25]. For completeness the equivalent temperatures are listed in table 3 for a specific load of 10 MPa and in table 4 for 5 MPa, respectively.

T_{TB} represents the equivalent temperature of the test bearing. T_{SB1} and T_{SB2} is the temperature for the support bearings. The maximum temperature difference between the test bearing and the two support bearings is around 2 °C. At 3000 rpm a maximum temperature of 108 °C for 10 MPa specific load is reached. At shaft speeds below 500 rpm the temperature remains similar within 0.6 °C for each bearing. Hence, an extensive heating due to asperity contact was not observed.

4.4 Surface roughness and contact pairs

The surfaces of bearing shell and shaft were scanned by a white light interferometer to determine the flow factors and the surface parameters for the contact pairs. Therefore measurement spots of a size of 1 mm by 1 mm were analyzed. The bearing shell was measured before the test run and for comparison a worn bearing shell was scanned. In combination with the shaft surface two contact pairs are generated (see table 5). The "new" contact pair combines the new bearing shell surface with the shaft surface. The "worn" contact pair represents the worn bearing shell surface. The hardened steel shaft is not subjected to any surface changes during the test. Therefore, the shaft surface parameters remain unchanged. The arithmetic average R_a of the bearing shell surface drops from 0.27 μm to 0.22 μm. The root mean square R_q decreases from 0.34 μm to 0.26 μm. Table 5 summarizes the parameters of the "new" and "worn" contact pair.

Specified are the arithmetic average of the surface

Table 3: Equivalent bearing temperatures at 10 MPa load

Speed [rpm]	150	200	250	300	400	500	1000	3000
T_{TB} [°C]	101.0	101.0	101.1	101.2	101.4	101.6	102.8	108.0
T_{SB1} [°C]	102.4	102.5	102.5	102.6	102.8	103.0	104.3	108.0
T_{SB2} [°C]	102.7	102.8	102.9	103.0	103.2	103.3	104.5	108.2

Table 4: Equivalent bearing temperatures at 5 MPa load

Speed [rpm]	150	200	250	300	400	500	1000	3000
T_{TB} [°C]	99.1	99.2	99.2	99.3	99.4	99.6	100.6	105.6
T_{SB1} [°C]	101.1	101.1	101.2	101.2	101.3	101.4	102.3	105.6
T_{SB2} [°C]	101.4	101.4	101.5	101.5	101.6	101.6	102.5	106.1

Table 5: Surface roughness and simulation input parameters for the test bearing shell and the shaft

Contact pair	New		Worn	
Surface	Shell	Shaft	Shell	Shaft
R_a [μm]	0.27	0.14	0.22	0.14
R_q [μm]	0.34	0.20	0.26	0.20
σ [μm]	0.28	0.13	0.23	0.13
δ [μm]	0.39	0.21	0.19	0.21
K [-]	0.001		0.002	
E^* [GPa]	53.3		53.3	
μ_{Bound} [-]	0.02		0.02	
Γ [-]	12	4	12	4

profile R_a, the root mean square of the profile R_q as well as the asperity summit roughness (root mean squared) σ and the mean summit height δ which both are relevant for the contact model in the simulation. The combined Young's modulus E^* and the elastic factor K are calculated according to section 4.2. A boundary friction coefficient μ_{Bound} of 0.02 is defined. Γ identifies the orientation of the asperities for each surface by the definition from Peklenik [44] which is used by Patir and Cheng:

$$\Gamma = \frac{\lambda_{0.5x}}{\lambda_{0.5y}}, \tag{10}$$

where $\lambda_{0.5x}$ and $\lambda_{0.5y}$ represents the autocorrelation length in circumferential and axial direction. If Γ is greater than one, as in the present case, the asperities are align with the circumferential direction.

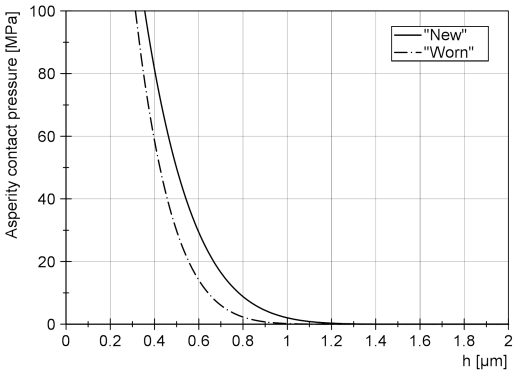

Figure 5: Calculated contact pressure according to equation 6 over oil film thickness for both contact pairs

Figure 5 shows the asperity contact pressure over the oil film thickness. The solid line represents the "new" contact pair which shows no contact until a lubrication gap below 1.2 μm. The contact pressure strongly increases with a further reduction of oil film thickness. The "worn" contact pair is shown as dash-dotted line. First asperity contact pressure can be identified around 1 μm. The increase of contact pressure is slightly steeper compared to the "new" contact pair because of the higher elastic factor K.

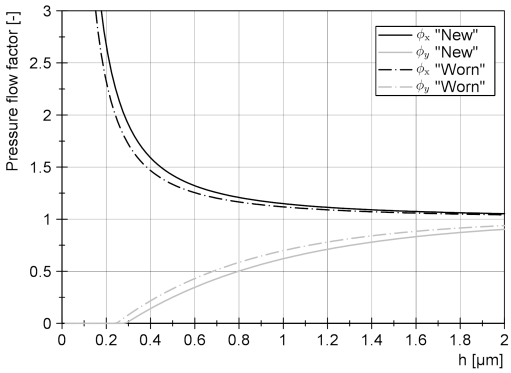

Figure 6: Pressure flow factors according to Patir and Cheng over oil film thickness for both contact pairs

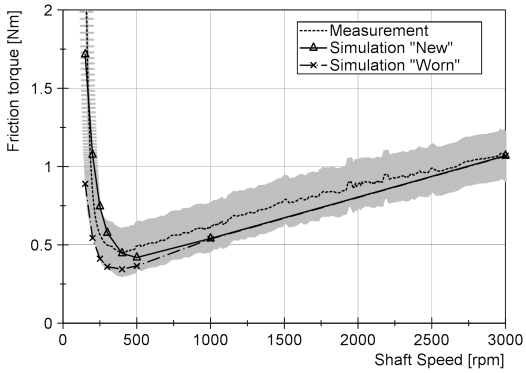

Figure 7: Comparison between calculated friction torque and measured friction torque over shaft speed at a load of 10 MPa.

The pressure flow factors in circumferential (x) and axial (z) direction for the two contact pairs are shown in figure 6. Both curves show an equal characteristics as the asperity orientation of the surfaces does not change but the curve of the "new" contact pair is slightly shifted to a higher lubrication gap h compared to the "worn" contact pair. The characteristic curves of the shear flow factor ϕ_s and the shear stress factors ϕ_f, ϕ_{fs} and ϕ_{fp} are shown in A.

5 Simulation results and validation

This section starts with a comparison between measurement and simulation and continues with a detailed discussion of the simulation results.

The dashed black curve in figure 7 shows the friction torque obtained from the measurement with a static load of 10 MPa. The grey area represents the uncertainty band of the torque and speed measurement. The other black lines represent the calculated friction torque, where the solid line refers to the "new" contact pair and the dash-dotted line to the "worn" contact pair. For both contact pairs the calculated friction torque at 1000 rpm and 3000 rpm are equal where all three bearings mainly operate in hydrodynamic regime. At 500 rpm and below, a higher friction torque is calculated for the "new" contact pair. However, both calculated friction curves lie within the measurement uncertainty. Regarding the position of minimum friction torque, the "worn" contact pair shows a good match to the measurement. The minimum friction torque occurs at 400 rpm.

Figure 8 shows the comparison between measurement and simulation similarly to previous the figure yet for a static load of 5 MPa. The beginning of pure hydrodynamic lubrication is shifted to a lower shaft speed at around 500 rpm. Again, the calculated friction torque is equal for both contact pairs in the hydrodynamic regime and matches the measured torque. As asperity contact occurs below 500 rpm the calculated friction torque differs between the two contact pairs. Obviously, the rougher "new" contact pair shows a higher friction torque compared to the "worn" contact pair. While the calculation results with the "new" contact pair lie within the measurement uncertainty for all speeds, the friction torque is slightly underestimated with the "worn" contact pair at low speed.

The calculated friction torque agrees with the measured friction torque for 5 MPa and 10 MPa over a wide range of operation. Hence, it can be concluded,

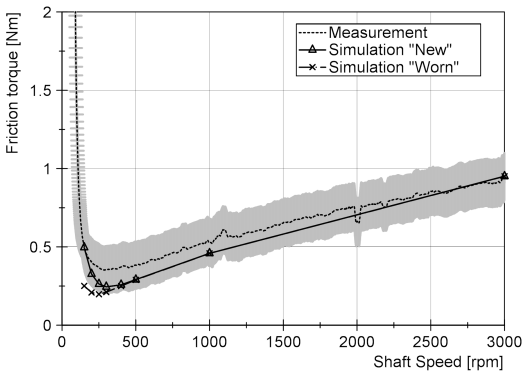

Figure 8: Comparison between calculated friction torque and measured friction torque over shaft speed at a load of 5 MPa.

that the presented method is suitable for lubricated journal bearings operating with intense asperity contact. Subsequently, the calculated results are further analyzed to discuss the influence of surface roughness on asperity contact pressure and friction losses. The case with a static load of 10 MPa is therefore exemplified.

First, the contributions of each bearing to the overall friction torque are of interest. Figure 9(a) shows the friction shares with the "new" contact pair applied. Correspondingly, figure 9(b) shows the results calculated with the "worn" contact pair. In the pure hydrodynamic lubrication regime, between 1000 rpm and 3000 rpm, the overall friction torque is equally distributed between all three bearings. By reducing the shaft speed, it can be identified, that asperity contact occurs primarily at the test bearing followed by the two support bearings. The bearing load per projected area is roughly three times higher at test bearing compared to the support bearings. As a result, the increase of friction moment with reducing shaft speed is mainly credited by the test bearing. Hence, the test bearing is mainly responsible for the sharp increase of the overall friction losses at lower speed.

By regarding the results of the two contact pairs it can be seen that the roughness influence is most notable at the higher stressed test bearing. Thus, the test bearing is further analyzed (see figure 10).

Figure 10(a) and figure 10(b) show the share of hydrodynamic friction torque and friction torque caused by asperity contact for the "new" and "worn" contact pair. The hydrodynamic friction torque decreases monotonically with decreasing shaft speed and is similar for both cases. Hence, the torque difference at shaft speeds at 500 rpm and below can be traced back to the friction caused by asperity contact only. The "new" contact pair shows a notable asperity friction torque at 500 rpm while it almost completely vanished for the "worn" contact pair. With a further speed reduction the torque caused by asperity contact steeply rises up to 1.25 Nm for the "new" contact pair at 150 rpm. In comparison the calculated maximum asperity friction torque for the "worn" contact pair reaches 0.6 Nm.

Additionally, the maximum hydrodynamic pressure and maximum asperity contact pressure which occurs in the lubrication gap are displayed as grey lines. The solid grey line represents the maximum hydrodynamic pressure. It nearly stays constant over the engine speed except at very low speed when it drops drastically, but first asperity contact pressure already occurs at higher shaft speed before the hydrodynamic pressure decreases. Therefore, the hydrodynamic pressure drop is not directly dependent to the occurrence of asperity contact. The maximum asperity contact pressure itself raises potentially with decreasing shaft speed. The deviation of maximum asperity contact pressure between the "new" and "worn" contact pair at the same speed is roughly 5 MPa. This deviation stays constant over the shaft speed.

The increase of friction moment in mixed lubrication is also dependent on the size of the area where asperity contact occurs. Figure 10(c) and figure 10(d) show the formation of asperity contact area for the "new" and "worn" contact pairs at three different shaft speeds. At 500 rpm (bottom figure) the asperity contact concentrates on the bearing edges only. This edge loading is caused by the elastic bending of the shaft for the presented case. However, a smaller size of contact area can be identified for the "worn"

contact pair. The results of the "new" contact pair at 250 rpm shows a contact area which spreads all along the bearing width. At the same speed, the contact area calculated with the "worn" contact model is still concentrated on the edges. At 150 rpm both contact pairs show asperity contact all along the bearing width.

Regarding to the above discussed maximum hydrodynamic pressure, the beginning of the pressure drop correlates to the speed where asperity contact pressure spreads over the whole bearing width for the first time. This is the case for both contact pairs.

The maximum asperity contact pressure remains at the bearing edge regardless of the shaft speed. It can also be identified that the circumferential position of the maximum asperity pressure moves towards the top position of the bearing with lower shaft speed. This behavior is best visible in figure 11 which shows the minimum radial distance between shaft and bearing shell and its corresponding circumferential position.

At a shaft speed of 3000 rpm the minimum radial displacement between shaft and bearing shell is 2 μm. The minimum distance occurs at 30° from the top position in other words, the shaft is shifted in circumferential direction with reference to the bearing shell. The minimum radial distance decreases with a drop in shaft speed. With figure 5 in mind asperity contact begins at around 1.2 μm for the "new" contact pair and 1.0 μm for the "worn" contact pair, respectively. The minimum radial distance as well as its circumferential position is exactly the same, as long as the bearing operates in hydrodynamic lubrication regime. Below 1 μm the radial distance distinguishes for the two contact pairs but the circumferential position remains similar. At 150 rpm the minimum radial distance, calculated with the "new" contact pair, is 0.7 μm. Using The "worn" contact pair results to a minimum radial distance of 0.6 μm. At 150 rpm the shaft has moved towards the top position of the bearing and stays at 10°.

6 Discussion

The simulation results match the measured Stribeck curve for the presented load cases. Especially at a specific load of 10 MPa, the results calculated with both contact pairs lie within the measurement uncertainty. Although, the calculated results with the "worn" contact pair show a clearly reduced friction torque in the mixed lubrication regime compared to the "new" contact pair. The detailed bearing results from previous section additionally estimate a reduced contact pressure, reduced size of contact area and a reduced minimum distance between shaft and bearing shell. Also the transition between hydrodynamic and mixed lubrication regime moves to a lower speed.

Regarding the transition speed, the "worn" contact pair appears to be more suitable at a specific load of 10 MPa. At 5 MPa the results with the "new" contact pair match the transition speed. It can be expected that an adaption of the surface roughness occur in the beginning of bearing operation. In the presented measurement procedure a speed up was performed before the Stribeck curve was determined. During the speed up metal-metal contact already occurs and a smoothing of the surface takes place. At higher specific load obviously higher metal-metal contact pressure develops and a quicker adaption of surface roughness can be expected. The quicker adaption at 10 MPa load eventually explains the good match of measurement and simulation with the "worn" surface roughness.

Nevertheless, the calculated friction benefit in mixed lubrication regime only considers the adaption of surface roughness due to running in. Beside the change of surface roughness, an adaption of the surface geometry occurs and effects the load carrying capacity of the fluid film. Additionally, a decrease in boundary friction coefficient with the running in progress can be expected which will further increase the friction benefit [45].

6.1 Boundary friction coefficient

A constant boundary friction coefficient μ_{Bound} is chosen for this model, although more complex models with a variable boundary friction coefficient ex-

ist [39]. The simplification bears the advantage that only a single variable has to be defined for a specific combination of bearing/shaft material and lubricant. The comparison between measurement and simulation show that the constant friction coefficient is suitable to predict friction in mixed lubrication regime where metal-metal contact is dominant in the high loaded region of the bearing. The results show a maximum asperity contact pressure of up to 20 MPa. Disadvantage of a single friction coefficient is the restriction to the mixed lubrication regime. In boundary lubrication regime, for instance the shaft starts to rotate, the friction torque is underestimated.

A change of μ_{Bound} does neither affect the friction losses in hydrodynamic regime nor impact the magnitude of asperity contact pressure. In fact it amplifies or reduces the friction torque caused by asperity contact (see equation 5). The transition speed between hydrodynamic and mixed lubrication stays exactly the same.

Nevertheless, friction in mixed lubrication is strongly dependent on film forming additives (friction modifier) added to the lubricant. The focus in the present work does not lie on the specification of lubricant additives but their influence should be mentioned as further research in this field is of interest. Spikes [46] identified three separate mechanisms in which lubricant additives can influence friction in mixed lubrication: (a) formation of a layer to reduce boundary friction at asperity contacts (b) formation of a thin film of high viscosity on the surface and (c) a change (reduction or increase) of effective surface roughness. Hence, for the friction prediction with different formulated engine oil an exclusively change of μ_{Bound} will may not provide satisfying result. Film forming additives in journal bearing application also enable a shift of the transition between hydrodynamic and mixed lubrication.

6.2 Influence of flow factors on friction torque

The presented results in previous section are calculated using the averaged Reynolds equation which considers the flow factors according to Patir and Cheng (see equation 2). The influence of neglecting the flow factors on the calculated friction torque is shown in figure 12.

The grey lines correspond to the calculated friction torque without considering the flow factors. The black lines include the flow factors in the calculation. The friction torque in pure hydrodynamic lubrication regime, above 1000 rpm, is not affected by the flow factors. By lowering the shaft speed and hence reducing the lubrication gap two changes when neglecting the flow factors can be identified. First the calculated friction torque in mixed lubrication regime increases notable without taking the flow factors into account. Second the transition between hydrodynamic and mixed lubrication moves slightly to a higher speed. However, the simulation results with the "worn" contact pair and without flow factors match the measurement over the observed speed range. The "new" contact pair overestimates the friction torque at low shaft speed.

7 Conclusion

This paper discusses journal bearing friction in mixed lubrication regime. For discussion purposes, measurements on a journal bearing test rig at KS Gleitlager were performed with two different static loads acting on the bearings. The measurement results provide a sound basis to validate the presented simulation approach. A detailed viscosity specification of the lubricant, dependent on temperature, pressure and shear rate, is included in the simulation model. The oil model has previously been validated for dynamic loads and a wide range of operation conditions [25]. The surface texture of the journal bearings have a major influence on friction in mixed lubrication regime. Hence, the surface of the state-of-the-art journal bearings are scanned and furthermore the flow factors, introduced by Patir and Cheng and parameters for the Greenwood and Tripp contact model are established.

The comparison of the friction torque between measurement and simulation show a good agreement in the hydrodynamic and mixed lubrication regime. Hence, the presented input data are suitable for the friction prediction in journal bearings operation un-

der severe conditions. The chosen constant boundary friction coefficient of $\mu_{\text{Bound}} = 0.02$ is appropriate for the presented combination of lubricant and bearing/shaft material. Both lubricant and material are current state of the art components used in modern combustion engines.

Furthermore, the simulation results are analyzed to discuss the influence of surface roughness on asperity contact and friction moment. A run-in surface roughness shows a lower maximum contact pressure and a reduced area of asperity contact compared to the roughness of a new bearing shell. A lower transition speed between hydrodynamic and mixed lubrication is identified. The run-in surface also predicts a smaller minimum distance between shaft and bearing shell.

8 Acknowledgment

We would like to express our gratitude to our supporting industrial and scientific project partners, namely KS Gleitlager, AVL and the Institute of Tribology of the TU Clausthal.

The authors would like to acknowledge the financial support of the "COMET - Competence Centers for Excellent Technologies Programme" of the Austrian Federal Ministry for Transport, Innovation and Technology (bmvit), the Austrian Federal Ministry of Science, Research and Economy (bmwfw), the Austrian Research Promotion Agency (FFG), the Province of Styria and the Styrian Business Promotion Agency (SFG).

Furthermore, we acknowledge the partial financial support of the Austrian Science Fund (FWF): P27806-N30.

9 References

References

[1] H. Spikes, Mixed lubrication–an overview, Lubrication Science 9 (3) (1997) 221–253.

[2] C. Taylor, Automobile engine tribology–design considerations for efficiency and durability, Wear 221 (1) (1998) 1–8.

[3] M. Priest, C. Taylor, Automobile engine tribology–approaching the surface, Wear 241 (2) (2000) 193–203.

[4] S. C. Tung, M. L. McMillan, Automotive tribology overview of current advances and challenges for the future, Tribology International 37 (7) (2004) 517–536.

[5] B. Jacobson, The stribeck memorial lecture, Tribology International 36 (11) (2003) 781–789.

[6] M. Woydt, R. Wäsche, The history of the stribeck curve and ball bearing steels: The role of adolf martens, Wear 268 (11) (2010) 1542–1546.

[7] C. Bovington, S. Korcek, J. Sorab, The importance of the stribeck curve in the minimisation of engine friction, Tribology Series 36 (1999) 205–214.

[8] X. Lu, M. Khonsari, An experimental investigation of dimple effect on the stribeck curve of journal bearings, Tribology Letters 27 (2) (2007) 169–176.

[9] J. Booker, S. Boedo, D. Bonneau, Conformal elastohydrodynamic lubrication analysis for engine bearing design: a brief review, Proceedings of the Institution of Mechanical Engineers-Part C: Journal of Mechanical Engineering Science 224 (12) (2010) 2648.

[10] M. B. Dobrica, M. Fillon, P. Maspeyrot, Mixed elastohydrodynamic lubrication in a partial journal bearing–comparison between deterministic and stochastic models, Journal of tribology 128 (4) (2006) 778–788.

[11] H.-C. Jao, K.-M. Chang, L.-M. Chu, W.-L. Li, A modified average reynolds equation for rough bearings with anisotropic slip, Journal of Tribology 138 (1) (2016) 011702.

[12] P. Tucker, P. Keogh, A generalized computational fluid dynamics approach for journal bearing performance prediction, Proceedings of the Institution of Mechanical Engineers, Part J: Journal of Engineering Tribology 209 (2) (1995) 99–108.

[13] H. Shahmohamadi, R. Rahmani, H. Rahnejat, C. P. Garner, D. Dowson, Big end bearing losses with thermal cavitation flow under cylinder deactivation, Tribology Letters 57 (2) (2015) 1–17.

[14] D. Bartel, Simulation von Tribosystemen, Vieweg, Wiesbaden (2010).

[15] G. Stachowiak, A. W. Batchelor, Engineering tribology, Butterworth-Heinemann, 2013.

[16] D. Bonneau, A. Fatu, D. Souchet, Mixed lubrication in hydrodynamic bearings, John Wiley & Sons, 2014.

[17] D. Bartel, L. Deters, Calculation of a stribeck curve of a journal bearing, Tribology series 36 (1999) 231–240.

[18] X. Lu, M. Khonsari, E. Gelinck, The stribeck curve: experimental results and theoretical prediction, Journal of tribology 128 (4) (2006) 789–794.

[19] S. Akbarzadeh, M. Khonsari, Effect of surface pattern on stribeck curve, Tribology letters 37 (2) (2010) 477–486.

[20] Y. Wang, Q. J. Wang, C. Lin, F. Shi, Development of a set of stribeck curves for conformal contacts of rough surfaces, Tribology transactions 49 (4) (2006) 526–535.

[21] D. Bartel, L. Bobach, T. Illner, L. Deters, Simulating transient wear characteristics of journal bearings subjected to mixed friction, Proceedings of the Institution of Mechanical Engineers, Part J: Journal of Engineering Tribology (2012) 1350650112454510.

[22] M. Fillon, J. Bouyer, Thermohydrodynamic analysis of a worn plain journal bearing, Tribology International 37 (2) (2004) 129–136.

[23] J. Bouyer, M. Fillon, I. Pierre-Danos, Influence of wear on the behavior of a two-lobe hydrodynamic journal bearing subjected to numerous startups and stops, Journal of Tribology 129 (1) (2007) 205–208.

[24] J. Sun, X. Zhu, L. Zhang, X. Wang, C. Wang, H. Wang, X. Zhao, Effect of surface roughness, viscosity-pressure relationship and elastic deformation on lubrication performance of misaligned journal bearings, Industrial Lubrication and Tribology 66 (3) (2014) 337–345.

[25] D. Sander, H. Allmaier, H. Priebsch, F. Reich, M. Witt, T. Füllenbach, A. Skiadas, L. Brouwer, H. Schwarze, Impact of high pressure and shear thinning on journal bearing friction, Tribology International 81 (2015) 29–37.

[26] N. Patir, H. Cheng, An average flow model for determining effects of three-dimensional roughness on partial hydrodynamic lubrication, ASME, Transactions, Journal of Lubrication Technology 100 (1978) 12–17.

[27] N. Patir, H. Cheng, Application of average flow model to lubrication between rough sliding surfaces, ASME, Transactions, Journal of Lubrication Technology 101 (1979) 220–230.

[28] J. Greenwood, J. Tripp, The contact of two nominally flat rough surfaces, Proceedings of the institution of mechanical engineers 185 (1) (1970) 625–633.

[29] H. Allmaier, C. Priestner, C. Six, H. Priebsch, C. Forstner, F. Novotny-Farkas, Predicting friction reliably and accurately in journal bearings–a systematic validation of simulation results with experimental measurements, Tribology International 44 (10) (2011) 1151–1160.

[30] H. Allmaier, C. Priestner, F. Reich, H. Priebsch, C. Forstner, F. Novotny-Farkas, Predicting friction reliably and accurately in journal bearings–the importance of extensive oil-models, Tribology International 48 (2012) 93–101.

[31] C. Priestner, H. Allmaier, H. Priebsch, C. Forstner, Refined simulation of friction power loss in crank shaft slider bearings considering wear in the mixed lubrication regime, Tribology International 46 (1) (2012) 200–207.

[32] H. Allmaier, C. Priestner, F. Reich, H. Priebsch, F. Novotny-Farkas, Predicting friction reliably and accurately in journal bearings - extending the simulation model to TEHD, Tribology International 58 (2013) 20–28.

[33] D. E. Sander, H. Allmaier, H. Priebsch, F. Reich, M. Witt, A. Skiadas, O. Knaus, Edge loading and running-in wear in dynamically loaded journal bearings, Tribology International 92 (2015) 395–403.

[34] H. Allmaier, D. Sander, H. Priebsch, M. Witt, T. Füllenbach, A. Skiadas, Non-newtonian and running-in wear effects in journal bearings operating under mixed lubrication, Proceedings of the Institution of Mechanical Engineers, Part J: Journal of Engineering Tribology (2015) 1350650115594191.

[35] H. Vogel, The law of the relation between the viscosity of liquids and the temperature, Phys. Z 22 (1921) 645–646.

[36] C. Barus, Isothermals, isopiestics and isometrics relative to viscosity, American journal of science (266) (1893) 87–96.

[37] M. M. Cross, Rheology of non-Newtonian fluids: a new flow equation for pseudoplastic systems, Journal of Colloid Science 20 (5) (1965) 417–437.

[38] G. Offner, Friction power loss simulation of internal combustion engines considering mixed lubricated radial slider, axial slider and piston to liner contacts, Tribology Transactions 56 (3) (2013) 503–515.

[39] G. Offner, O. Knaus, A generic friction model for radial slider bearing simulation considering elastic and plastic deformation, Lubricants 3 (3) (2015) 522–538.

[40] G. Offner, Modelling of condensed flexible bodies considering non-linear inertia effects resulting from gross motions, Proceedings of the Institution of Mechanical Engineers, Part K: Journal of Multi-body Dynamics 225 (3) (2011) 204–219.

[41] J. Krasser, Thermoelastohydrodynamische Analyse dynamisch belasteter Radialgleitlager, Ph.D. thesis, Technische Universität Graz (1996).

[42] B. Jakobsson, L. Floberg, The finite journal bearing considering vaporization, Transactions of Chalmers University of Technology, 1957.

[43] J. Greenwood, J. Williamson, Contact of nominally flat surfaces, Proceedings of the Royal Society of London. Series A, Mathematical and Physical Sciences 295 (1966) 300–319.

[44] J. Peklenik, Paper 24: New developments in surface characterization and measurements by means of random process analysis, in: Proceedings of the Institution of Mechanical Engineers, Conference Proceedings, Vol. 182, SAGE Publications, 1967, pp. 108–126.

[45] P. J. Blau, On the nature of running-in, Tribology International 38 (11) (2006) 1007–1012.

[46] H. Spikes, Film-forming additives-direct and indirect ways to reduce friction, Lubrication Science 14 (2) (2002) 147–167.

A Shear flow factor and shear stress factors

The shear flow factor ϕ_s and the shear stress factors ϕ_f, ϕ_{fs} and ϕ_{fp} are shown in figure 13, 14 and 15. Each diagram compares the "new" and the "worn" contact model.

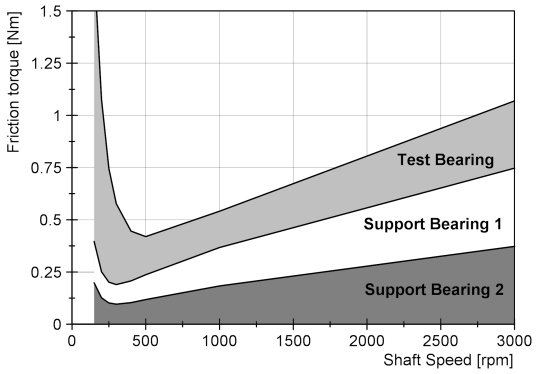

(a) "New" contact pair

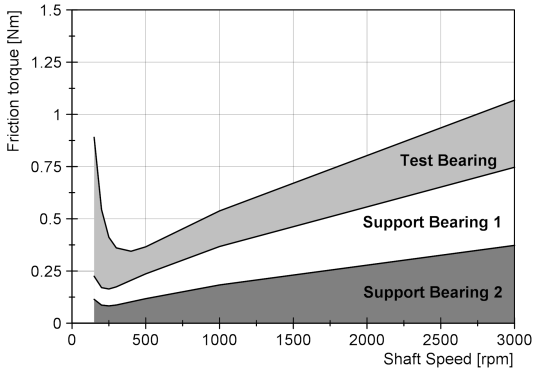

(b) "Worn" contact pair

Figure 9: Calculated friction contribution of each bearing at 10 MPa load

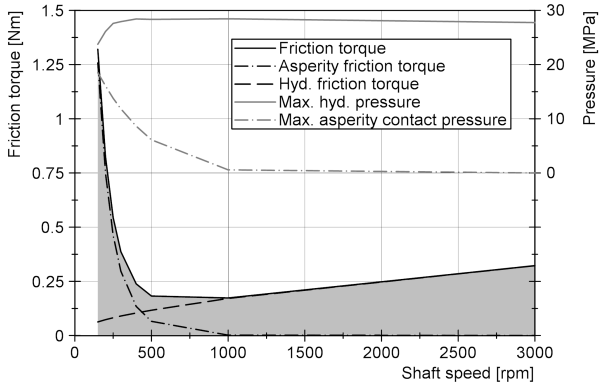

(a) "New" contact pair, friction contribution and maximum pressure

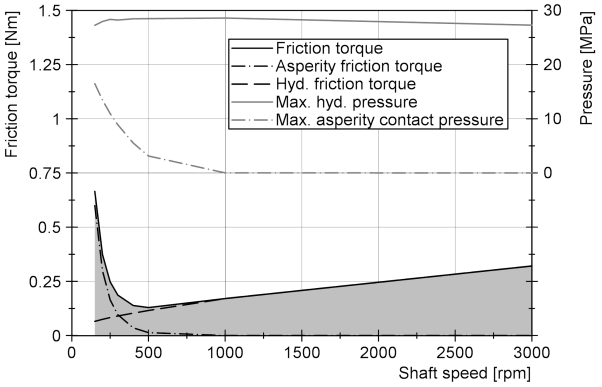

(b) "Worn" contact pair, friction contribution and maximum pressure

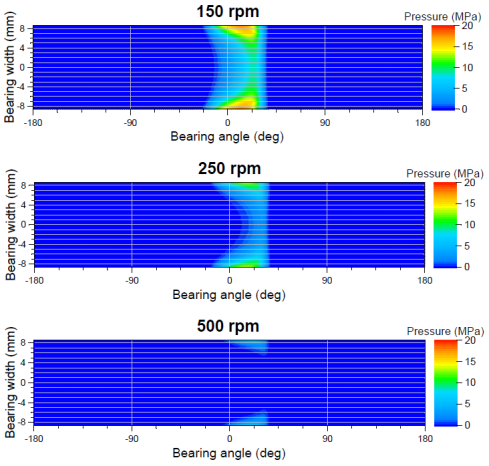

(c) "New" contact pair, asperity contact pressure distribution at different shaft speeds

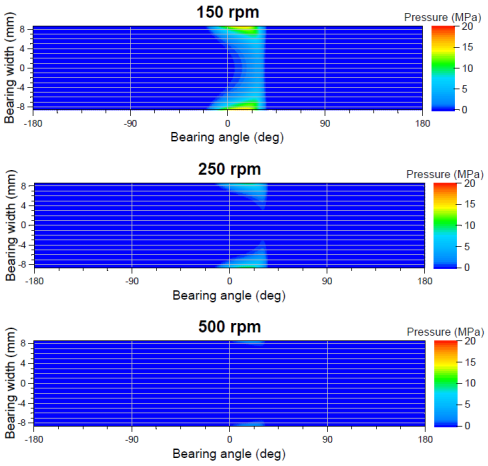

(d) "Worn" contact pair, asperity contact pressure distribution at different shaft speeds

Figure 10: Specific analysis of the test bearing simulation results, 10 MPa load

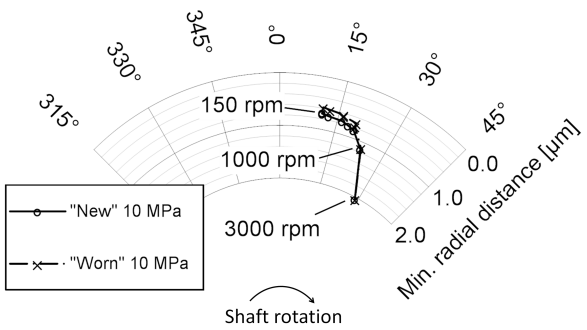

Figure 11: Minimum radial distance between shaft and bearing shell and its circumferential position

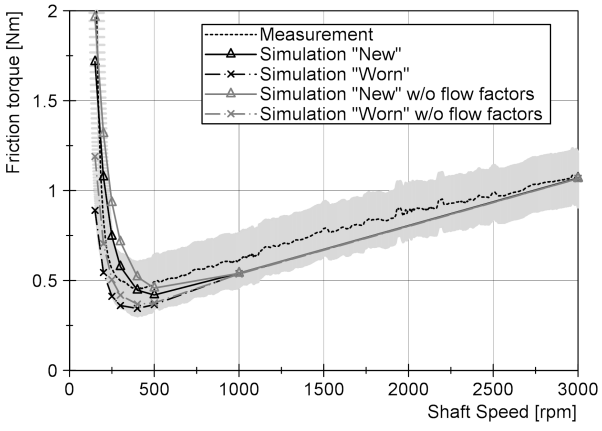

Figure 12: Influence of flow factors on friction prediction at 10 MPa load.

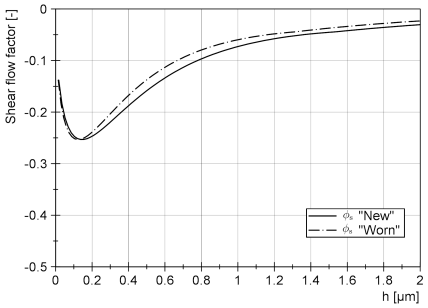

Figure 13: Shear flow factor according to Patir and Cheng over oil film thickness for both contact pairs

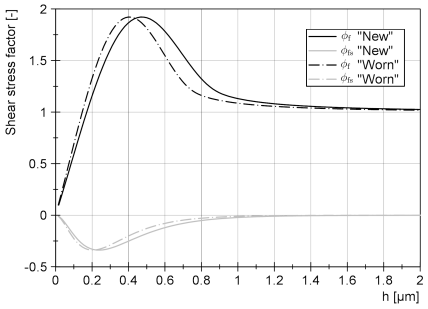

Figure 14: Shear stress factor according to Patir and Cheng over oil film thickness for both contact pairs

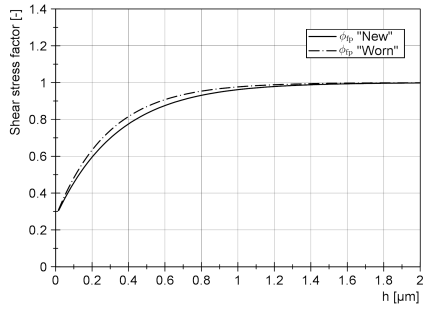

Figure 15: Shear stress factor according to Patir and Cheng over oil film thickness for both contact pairs